Substituent-Induced Circular Dichroism in Phthalocyanines

Nagao Kobayashi,*,† Ryuji Higashi,† Bruno C. Titeca,‡ Folker Lamote,‡ and Arnout Ceulemans*,‡

Contribution from the Department of Chemistry, Graduate School of Science, Tohoku University, Sendai 980-8578, Japan, and Division of Quantum Chemistry, University of Leuven, Celestijnenlaan 200F, B-3001 Leuven, Belgium

Received July 19, 1999

Abstract: Phthalocyanines with two and four optically active binaphthyl units have been synthesized and characterized by electronic absorption, CD, and MCD spectroscopy. The chiral substituents induce CD in the in-plane polarized Q and Soret bands of phthalocyanines: phthalocyanines having *R* and *S* binaphthyls show positive and negative CD, respectively. The geometries of the compounds were optimized at the PM3 level, and a vector coupling model for the induction of rotatory strength was developed. This model provides a semi-quantitative description of the CD spectra. Thus, not only the sign of the CD spectra but also the intensity relationship between the Soret and Q CD bands and, further, the shape of the Q CD band were reasonably explained. The discussion focuses on the important role of the central hydrogen atoms.

1. Introduction

Large aromatic ring systems such as phthalocyanines and porphyrins have characteristic $\pi - \pi^*$ absorption bands in the UV−vis region that are in-plane polarized and therefore intrinsically achiral.[1] Chirality is induced by introducing substituents on the periphery of the ring. The induced rotatory strength can be estimated on the basis of a coupled-oscillator model, which provides information on the local environment of the chromophore. As an example, Woody et al.[2] have used this model to investigate the origin of the heme Cotton effect in myoglobin and hemoglobin, and Mitzutani et al.[3] observed induced CD in zinc porphyrins with naphthyl substituents. In these cases, both the chromophore and the substituent are achiral, and the rotatory strength can only arise when the perturber has an electric transition moment which is skewed with respect to the moment on the ring system. A different induction channel is opened when the perturber itself exhibits a strong circular dichroism, which can directly be transferred to the ring system by a CD stealing mechanism.

To investigate this mechanism we have synthesized several phthalocyanine (Pc) compounds with chiral binaphthyl substituents.[4] The distance between the chiral binaphthyl units and the Pc core was shortened compared with our previous similar compounds.[5] This enhances the induced rotational strength and facilitates a quantitative comparison between theory and experiment.

In the theoretical part of the paper, we derive expressions for the CD of Pc with a single binaphthyl substituent and then extend the results to polysubstituted compounds. The conclusions have implications for the design of magneto-optic materials[6] and the interpretation of Fluorescence Detected Circular Dichroism (FDCD) in proteins.[7]

2. The Induction Mechanisms for Circular Dichroism in Achiral Electric Dipole Transitions

Consider a phthalocyanine chromophore, i, with a characteristic electric dipole-allowed transition at energy $h\nu_i$ and transition moment $\boldsymbol{\mu}_i$. The associated magnetic transition moment $\mathbf{m}_i$ is taken to be strictly symmetry-forbidden, as is the case for the in-plane polarized $^1A_{1g} \rightarrow {}^1E_u$ transition in phthalocyanine. On i we place a chiral substituent, j, such as binaphthyl, which exhibits a strong optically active transition at energy $h\nu_j$ with electric transition moment $\boldsymbol{\mu}_j$ and magnetic transition moment $\mathbf{m}_j$.

For the theoretical treatment we will adopt the SI units[8] with ν in s^{-1}, $\boldsymbol{\mu}$ in m C, $\mathbf{m}$ in $m^2\ s^{-1}$ C, and rotatory strength in $m^3\ s^{-1}\ C^2$.

Perturbation theory provides two predominant mechanisms[9−11] to induce circular dichroism in the transition on i: the Kuhn-Kirkwood coupled oscillator mechanism and the CD stealing term. The rotatory strength of the coupled oscillator mechanism in SI units is given by

$$R_1 = -\frac{2\pi\nu_i\nu_j V_{ij}}{h(\nu_j^2 - \nu_i^2)}(\mathbf{r}_j - \mathbf{r}_i)\cdot(\boldsymbol{\mu}_j \times \boldsymbol{\mu}_i) \qquad (1)$$

where $\mathbf{r}_i$ and $\mathbf{r}_j$ are the position vectors of the centers of gravity of *i* and *j*. V_{ij} is the dipole−dipole interaction element which

* Address correspondence to either author: (e-mail) nagaok@mail.cc.tohoku.ac.jp; arnout.ceulemans@chem.kuleuven.ac.be.

† Tohoku University.

‡ K. U. Leuven.

(1) Stillman, M. J. In *Phthalocyanines, Properties and Applications*; Leznoff, C. C., Lever, A. B. P., Eds.; VCH Publishers: New York, 1989; pp 133−289.

(2) Hsu, M.-C.; Woody, R. W. *J. Am. Chem. Soc.* **1971**, *93*, 3515−3525.

(3) Mitzutani, T.; Ema, T.; Yoshida, T.; Kuroda, Y.; Ogoshi, H. *Inorg. Chem.* **1993**, *32*, 2072−2077.

(4) Kobayashi, N. *Chem. Commun.* **1998**, 487−488.

(5) Kobayashi, N.; Kobayashi, Y.; Osa, T. *J. Am. Chem. Soc.* **1993**, *115*, 10994−10995.

(6) Fox, J. M.; Katz, T. J.; Van Elshocht, S.; Verbiest, T.; Kauranen, M.; Persoons, A.; Thongpanchang, T.; Krauss, T.; Brus, L. *J. Am. Chem. Soc.* **1999**, *121*, 3453−3459.

(7) Lobenstine, E. W.; Schaefer, W. C.; Turner, D. H. *J. Am. Chem. Soc.* **1981**, *103*, 4936−4940.

(8) IUPAC, Physical Chemistry Division. *Quantities, Units and Symbols in Physical Chemistry*; Mills, I., Cvitaš, T., Homann, K., Kallay, N., Kuchitsu, K., Eds.; Blackwell: Oxford, 1988.

(9) Tinoco, I. *Adv. Chem. Phys.* **1962**, *4*, 113−160.

(10) Schipper, P. E. *J. Am. Chem. Soc.* **1979**, *101*, 6826−6829.

(11) Rodger, A.; Nordén, B. *Circular Dichroism and Linear Dichroism*; Oxford University Press: Oxford, 1997.

10.1021/ja992556w CCC: $18.00
Published on Web 12/11/1999

couples the two transitions

$$V_{ij} = \frac{1}{4\pi\epsilon_0}\left(\frac{\boldsymbol{\mu}_i\cdot\boldsymbol{\mu}_j}{|\mathbf{r}_j - \mathbf{r}_i|^3} - \frac{3(\boldsymbol{\mu}_i\cdot(\mathbf{r}_j - \mathbf{r}_i))(\boldsymbol{\mu}_j\cdot(\mathbf{r}_j - \mathbf{r}_i))}{|\mathbf{r}_j - \mathbf{r}_i|^5}\right) \quad (2)$$

where ϵ_0 is the permittivity of vacuum. In this mechanism rotatory strength can arise if the electric transition dipoles on the chromophore and on the substituent are skewed. This implies a sensitive dependence on the actual geometry of the complex.

The other CD stealing mechanism directly transfers rotatory strength from the strongly active substituent to the central transition, again via dipolar coupling:

$$R_2 = -\frac{2\nu_i V_{ij}}{h(\nu_j^2 - \nu_i^2)}\,\mathrm{Im}(\boldsymbol{\mu}_i\cdot\mathbf{m}_j) \quad (3)$$

where Im denotes the imaginary part of. This mechanism also is strongly geometry-dependent. It requires the transition moments at the two centers to be aligned.

A possible third mechanism would be the coupling between the magnetic transition moment of the central chromophore and the electric transition moments of the periphery. In the D_{4h} symmetry group of the unsubstituted metallo-phthalocyanine, transitions to both Soret and *Q* bands transform as E_u representations, while magnetic transition moments require $E_g + A_{2g}$ symmetries. Hence, neither of the Pc transitions carries an intrinsic magnetic moment. Therefore, in a coupled chromophore model, this third mechanism is strictly symmetry-forbidden.

3. Synthesis and Spectroscopy

In this paper we study in detail phthalocyanine complexes with two and four binaphthyl substituents. The bisubstituted complexes **1** have oxo bridges and will be denoted as BNpPcM, with M = H_2, Zn, Co. The tetrasubstituted complexes **2** are linked to the outer benzo groups by sulphur bridges and are denoted as TNpPcM (M = H_2, Zn, Co). Monosubstituted

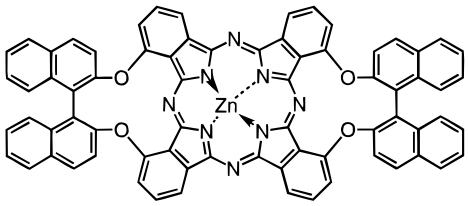

1

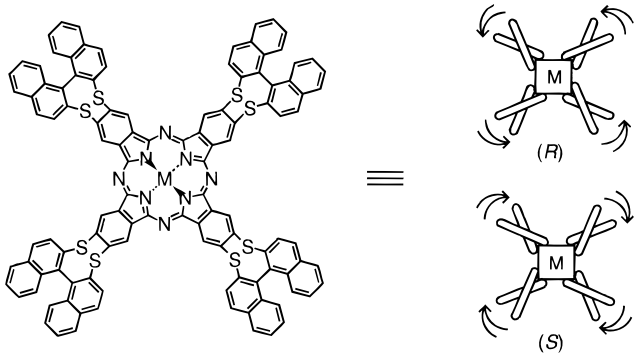

2

complexes have also been reported in a preliminary communication.[4] The configuration of the binaphthyl is further indicated as *R* or *S*, following the standard convention. Typical absorption, CD, and MCD spectra are shown in Figures 1−3. The spectra show the characteristic phthalocyanine Q and Soret bands at about 700 and 370 nm, respectively. In the CD spectra, the *R* and *S* binaphthyl-linked phthalocyanines show positive and negative CD, respectively, corresponding to these bands. In the far UV one observes in Figures 2 and 3 the strongly dichroic absorptions of the binaphthyl.

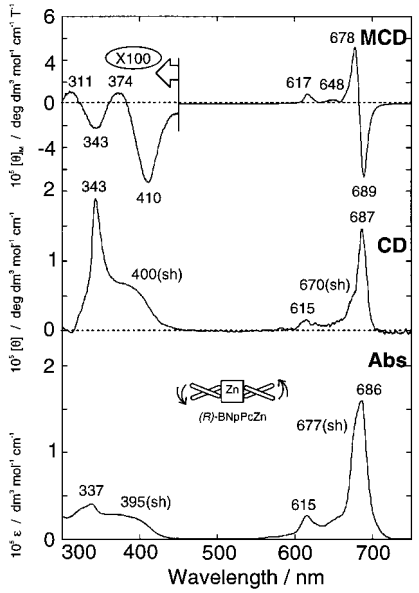

Figure 1. Spectra for (*R*)-BNpPcZn in DMF.

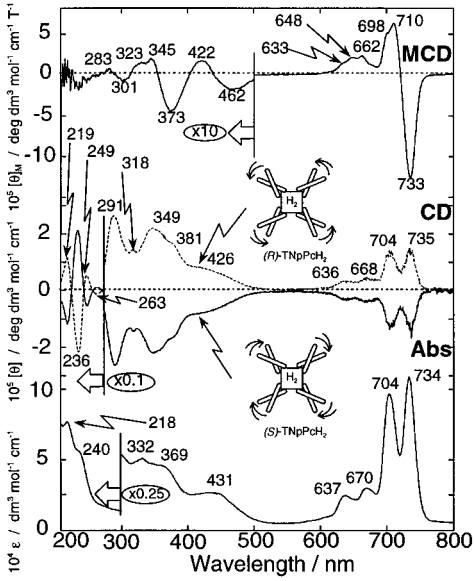

Figure 2. Spectra for $TNpPcH_2$ in THF.

The oscillator strength, *f*, of an electronic transition with energy $h\nu$ and transition dipole $\boldsymbol{\mu}$ is defined as[11,12]

$$f = \frac{4\pi m_e}{3\hbar e^2}\,\nu\,|\boldsymbol{\mu}|^2 \quad (4)$$

This is a dimensionless quantity which may be related to the integrated absorption band:

(12) Michl, J.; Thulstrup, E. W. *Spectroscopy with Polarized Light*; VCH Publishers: New York, 1986.

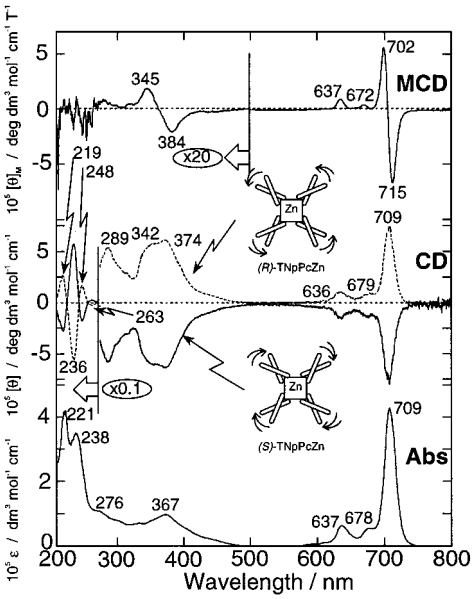

Figure 3. Spectra for TNpPcZn in THF.

$$f = \frac{4m_e c\epsilon_0 \ln 10}{10N_A e^2} \int \epsilon(\bar{\nu})\, \mathrm{d}\bar{\nu} \qquad (5)$$

Here $\epsilon(\bar{\nu})$ is the extinction coefficient in its usual non SI units of dm^3 mol^{-1} cm^{-1}; $\bar{\nu}$ is the wavenumber, $\bar{\nu} = \nu/c$. The Q bands in phthalocyanines typically have two strong vibrational satellites at distances of ~650 and 1600 cm^{-1} from the main peak (see, e.g., Figure 3). These are usually assigned as vibronic sidebands, which gain intensity via Herzberg-Teller coupling[1,13] rather than via a Franck-Condon mechanism. They do not contribute to the oscillator strength of the electronic transition and should thus be excluded from the integration. To avoid overlap with these bands, a Gaussian band fit was performed on the main peak:

$$\epsilon(\bar{\nu}) = \sum_k \epsilon^k_{\max} \exp\left(\frac{-4 \ln 2\, (\bar{\nu} - \bar{\nu}^k_{\max})^2}{(\Delta\bar{\nu}^k_{1/2})^2}\right) \qquad (6)$$

$\Delta\bar{\nu}_{1/2}$ is the band width at half maximum. The integrated absorption then is given by:

$$\int \epsilon(\bar{\nu})\, \mathrm{d}\bar{\nu} = \sum_k \frac{\sqrt{\pi}}{2\sqrt{\ln 2}} \epsilon^k_{\max} \Delta\bar{\nu}^k_{1/2} \qquad (7)$$

The results of this analysis are given in Table 1. In most cases the Q(0,0) band could be described by a single Gaussian curve. The fit of the UV bands in TNpPcZn is shown in Figure 4. The final column in Table 1 lists the empirical estimates of the transition dipoles based on the spectral fit. These quantities will further be used in the theoretical analysis. Note that dipoles have been given in the usual Debye units: 1 D = 3.33564 × 10^{-30} Cm.

The CD spectra record the molar ellipticity, $[\theta]$, given in deg dm^3 mol^{-1} cm^{-1}. This quantity is a measure for the difference between extinction coefficients for left and right circulary polarized light:

$$[\theta] = \frac{4500 \ln 10}{\pi} (\epsilon_l - \epsilon_r) \qquad (8)$$

The rotatory strength, R, of a transition is related to the integrated ellipticity according to:

$$R = \frac{3c^2\epsilon_0\hbar \ln 10}{40\pi N_A} \int \frac{\epsilon_l(\bar{\nu}) - \epsilon_r(\bar{\nu})}{\bar{\nu}}\, \mathrm{d}\bar{\nu}$$

$$= \frac{c^2\epsilon_0\hbar}{6 \times 10^4 N_A} \int \frac{[\theta(\bar{\nu})]}{\bar{\nu}}\, \mathrm{d}\bar{\nu} \qquad (9)$$

An almost perfect integration could be performed by direct Gaussian expansion of the $[\theta]/\bar{\nu}$ function. The resulting R values are given in Table 2. According to standard practice, the rotatory strengths are given in units of Debye times Bohr magneton: 1 Dμ_B = 3.0935 × 10^{-53} m^3 s^{-1} C^2. In Figures 5 and 6 the spectral fits of the Q-band and UV-bands for (R) − TNpPcZn are shown.

We have also recorded MCD spectra. Those of TNpPcZn and TNpPcCo have a clear derivative shape in the Q and Soret regions (Faraday A terms), which is characteristic of transitions to orbitally degenerate states.[1] The spectra of metal-free

Table 1. Results of the Gaussian Fit Analysis (Absorption Spectra)

complex		$\bar{\nu}^k_{\max}$ (cm^{-1})	$\epsilon^k_{\max}$ (dm^3/mol cm)	$\Delta\bar{\nu}^k_{1/2}$ (cm^{-1})	f (/)	$\lvert\boldsymbol{\mu}\rvert$ (D)
BNpPcZn	$Q(0,0)$	14 611	158 313	445.5	0.3495	7.128
		14 866	25 845	212.0		
TNpPcZn	$Q(0,0)$	14 162	421 715	409.4	0.7939	10.919
	UV	43 070	339 359	4765.6	7.4356	19.162
		47 243	369 549	3414.5	5.8015	16.161
BNpPcCo	$Q(0,0)$	14 679	68 149	759.4	0.2379	5.872
TNpPcCo	$Q(0,0)$	14 022	150 846	514.7	0.4023	7.799
		14 446	28 639	344.6		

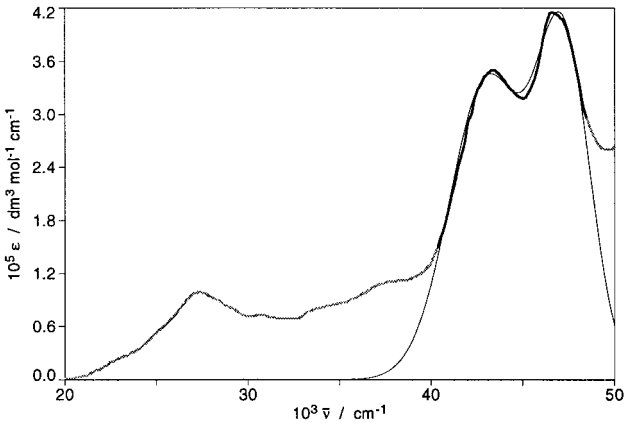

Figure 4. Fit of the UV bands in TNpPcZn.

Table 2. Results of the Gaussian Fit Analysis (CD Spectra)

complex		$\bar{\nu}^k_{\max}$ (cm^{-1})	$(\theta(\bar{\nu})/\bar{\nu})^k_{\max}$ (deg dm^3/mol)	$\Delta\bar{\nu}^k_{1/2}$ (cm^{-1})	R (Dμ_B)
(R)-BNpPcZn	$Q(0,0)$	14 544	9.63	264.0	0.2740
		14 856	2.84	311.7	
(R)-TNpPcZn	$Q(0,0)$	14 191	51.56	417.2	1.7188
	UV	43 696	−122.0	2315.6	−22.5748
		47 373	50.70	2983.7	12.0895
(R)-BNpPcCo	$Q(0,0)$	14 444	2.19	313.8	0.1655
		14 717	2.52	548.9	
(R)-TNpPcCo	$Q(0,0)$	14 015	15.38	581.9	0.7150

(13) Braun, D.; Ceulemans, A. In *AIP Conference Proceedings of the Fast Elementary Processes in Chemical and Biological Systems. 54th Int. Meeting of Physical Chemistry*, Tramer, A., Ed.; Woodbury: New York, 1996; no. 364, pp 211−216.

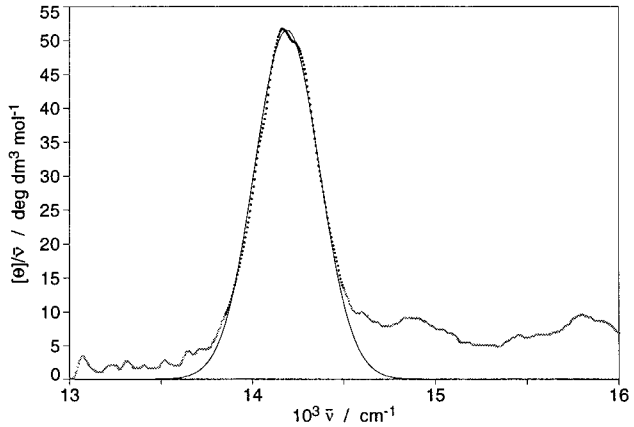

Figure 5. Fit of the Q band in (*R*)-TNpPcZn.

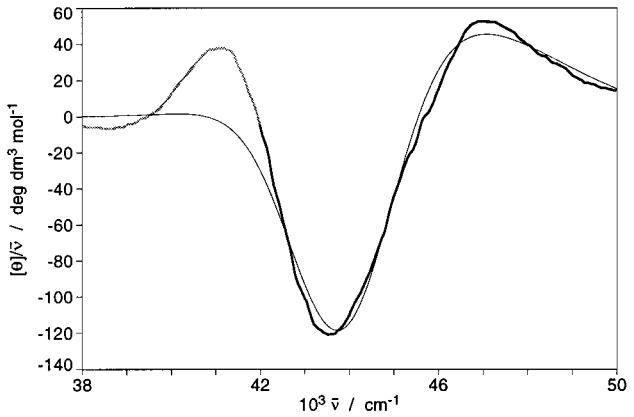

Figure 6. Fit of the UV bands in (*R*)-TNpPcZn.

derivatives result from a superposition of Faraday *B* terms,[14] which arise from the mixing of states by the magnetic field. The MCD spectrum of BNpPcZn appears to contain a pseudo-*A* term (for more details, see Discussion). For earlier theoretical work on the MCD of porphyrin and related chromophores, see refs 15−18.

4. Geometry Optimization

To determine the geometrical parameters that are required in the expressions for the rotatory strength, a geometry optimization has been carried out at the PM3 level. Both the disubstituted compound with oxygen bridges and the tetrasubstituted compound with sulphur bridges were optimized.

For (*R*)-BNpPcH$_2$, the phthalocyanine system was kept planar, and a twofold symmetry axis perpendicular to this plane was imposed. The resulting geometry is shown in Figure 7a. It has the two binaphthyl units in the *R* configuration. A Cartesian (*x*, *y*, *z*) coordinate frame was defined with the *z* axis normal to the plane and the *y* direction through the substituents. On the binaphthyl unit on the right a further (x', y', z') system is defined with the x' axis along the internaphthyl bond. This is shown more clearly in Figure 8. The *y* and y' directions coincide. If the central hydrogens are replaced by a metal ion, the point group symmetry can be as high as D_2, with twofold axes along the three Cartesian directions. In the subsequent theoretical

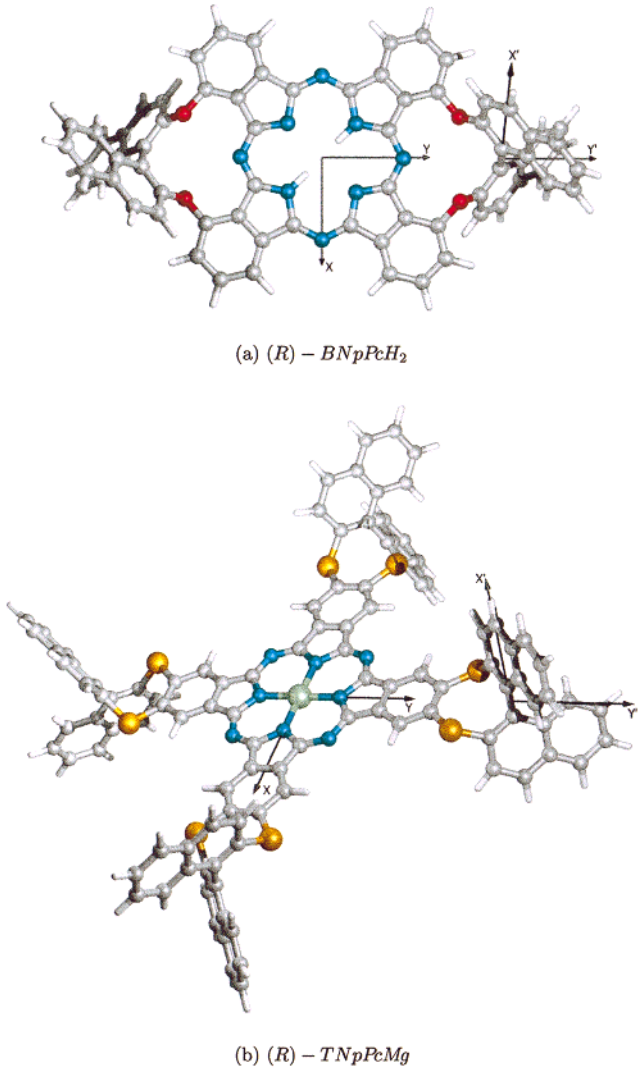

Figure 7. Optimized geometries.

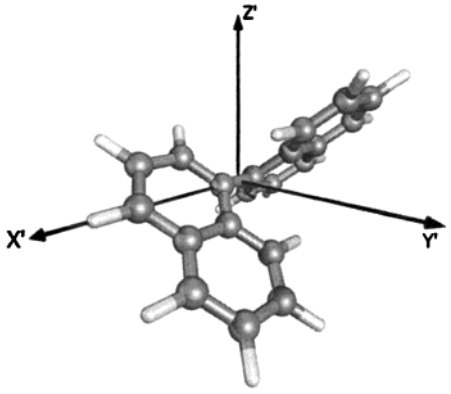

Figure 8. Binaphthyl unit.

model the C_2^y symmetry element, which bissects both the i and j systems, appears to be very useful. The central hydrogens will break this symmetry. An assessment of their influence on the CD spectrum will be postponed till the Discussion.

Also (*R*)-TNpPcM (with M = Mg) was optimized in tetragonal D_4 symmetry. In this case, preliminary optimization of separate fragments was required in order to reach convergence for the whole macromolecule. The resulting geometry is shown in Figure 7b. A Cartesian axes system is also defined. Note that *x* and *y* directions are now running through the pyrrole nitrogens. The local (x', y', z') system on the binaphthyls follows

(14) Tajiri, A.; Winkler, J. *Z. Naturforsch., A: Phys. Sci.* **1983**, *38a*, 1263−1269.
(15) Ceulemans, A.; Oldenhof, W.; Görller-Walrand, C.; Vanquickenborne, L. G. *J. Am. Chem. Soc.* **1986**, *108*, 1155−1163.
(16) Michl, J. *J. Am. Chem. Soc.* **1978**, *100*, 6801−6811.
(17) Michl, J. *J. Am. Chem. Soc.* **1978**, *100*, 6812−6818.
(18) Waluk, J.; Michl, J. *J. Org. Chem.* **1991**, *56*, 2729−2736.

Table 3. Relevant Geometrical Parameters and Optimized Values for the Di- and Tetra-Substituted Pcs Shown in Figure 7a,b (see also Figure 9)

	$BNpPcH_2$	TNpPcMg
R_{12}	8.62 Å	11.14 Å
r_{12}	4.33 Å	4.30 Å
α	82.58°	73.74°
θ	55.42°	67.72°

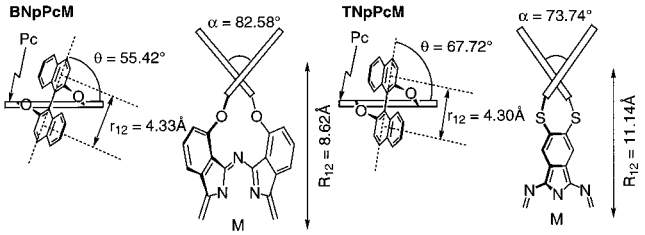

Figure 9. Parameters used in Table 3.

exactly the same definition as before, since the binaphthyl unit is similar in both compounds.

For the further treatment, the following geometrical parameters are important: (i) the distance, R_{12}, between the centers of gravity of Pc and of the binaphthyl substituent, (ii) the internaphthyl distance, r_{12}, between the centers of the hexagons along the x' direction, (iii) the dihedral angle, α, between the naphthyl planes, and (iv) the inclination, θ, of the internaphthyl bond with respect to the Pc plane. Table 3 provides the numerical values that were extracted from the calculation. The parameters are also shown in Figure 9. The dihedral angle between the naphthalene planes is close to a right angle. The same result is found in the case of the free binaphthyl, $C_{20}H_{14}$, and is due to steric hindrance between the naphthalene planes. The distance between the centers of the chromophore and the substituent is larger in $TNpPcH_2$ than in $BNpPcH_2$. This simply reflects the different substitution modes in the two compounds.

5. The Theoretical Model

5.1 The Circular Dichroism of Binaphthyl. The first step in the construction of the theoretical model concerns the optical activity of the isolated binaphthyl group. A simple Kuhn-Kirkwood coupled oscillator model has been demonstrated to provide the required rationale for the optical activity of several biaryl-type compounds, including our binaphthyl substituents.[19] We will briefly revisit this model, since it will instruct us how the $\boldsymbol{\mu}_j$ and $\mathbf{m}_j$ moments are oriented and indicate what level of understanding can be expected.

The optical activity of the binaphthyl is associated with the long-axis polarized B_b transition of the naphthyl units, with frequency ν_N. The equisymmetric L_b transition is three orders of magnitude less intense and can thus safely be neglected. In addition, naphthalene has, below 40 000 cm^{-1}, a short-axis polarized L_a transition, which is one order of magnitude less intense than B_b. This transition has no intrinsic chirality and therefore cannot contribute to the CD stealing mechanism. In principle, it could add a minor contribution to the Kuhn-Kirkwood coupled oscillator model, but the actual geometry is not favorable for such a mechanism—the angle θ between its direction of polarization and the Pc plane being closer to 90° (see Table 3). For those reasons we will only consider the B_b transitions.

Figure 8 shows the so-called *R* configuration. Let $\boldsymbol{\mu}_1$ and $\boldsymbol{\mu}_2$ denote the individual long-axis polarized moments on the naphthyls. These moments form a screw with a propeller angle which is equal to the dihedral angle α between the two naphthyl planes. **3** offers a view of the moments in the local Cartesian

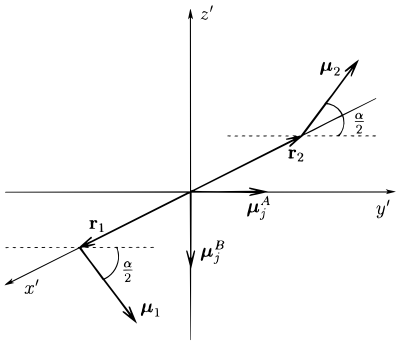

3

($x'y'z'$) frame with the origin in the center of the binaphthyl bridge. In this frame the moments are described as follows

$$\boldsymbol{\mu}_1 = \mu_N\left(\cos\frac{\alpha}{2}\,\mathbf{e}_{y'} - \sin\frac{\alpha}{2}\,\mathbf{e}_{z'}\right) \tag{10}$$

$$\boldsymbol{\mu}_2 = \mu_N\left(\cos\frac{\alpha}{2}\,\mathbf{e}_{y'} + \sin\frac{\alpha}{2}\,\mathbf{e}_{z'}\right) \tag{11}$$

where μ_N denotes their length, and the **e** symbols are unit vectors along the specified directions; $\mathbf{r}_1$ and $\mathbf{r}_2$ are two vectors directed to the centers of the hexagons that are bridged. The distance $|\mathbf{r}_1 - \mathbf{r}_2|$ will be denoted as r_{12}. The excitonic eigenstates correspond to the normalized sum and difference combinations of the two transitions. They are respectively symmetric (*A*) and antisymmetric (*B*) with respect to the twofold axis through the central bridge. The corresponding transition moments are given by:

$$\boldsymbol{\mu}_j^A = (\boldsymbol{\mu}_1 + \boldsymbol{\mu}_2)/\sqrt{2} \tag{12}$$

$$\boldsymbol{\mu}_j^B = (\boldsymbol{\mu}_1 - \boldsymbol{\mu}_2)/\sqrt{2} \tag{13}$$

The separation between the two states amounts to:

$$E_j^A - E_j^B = 2V_{12} \tag{14}$$

where V_{12} represents the interaction element which transfers the excitation. The dipole coupling approximation probably does not provide a reliable estimate of this interaction element, in view of the short distance between the naphthyls. From a study by Mason and Grinter[20] on the analogous 1,1-bianthryls, it seems to be well established that for dihedral angles close to 90° the symmetric *A* component will be the upper state. The electric moment for this state can be expressed as:

$$\boldsymbol{\mu}_j^A = \sqrt{2}\mu_N \cos\frac{\alpha}{2}\,\mathbf{e}_{y'} \tag{15}$$

The coupling of the two naphthyl oscillators in this state also generates a magnetic moment, $\mathbf{m}_j^A$, which is given by:

(19) Krow, G. *Top. Stereochem.* **1970**, *5*, 31−68.
(20) Grinter, R.; Mason, S. F. *Trans. Faraday. Soc.* **1964**, *60*, 274−284.

$$\mathbf{m}_j^A = \frac{\pi\imath\nu_N}{\sqrt{2}}(\mathbf{r}_1 \times \boldsymbol{\mu}_1 + \mathbf{r}_2 \times \boldsymbol{\mu}_2)$$

$$= \frac{\pi\imath\nu_N \mu_N}{\sqrt{2}} r_{12} \sin\frac{\alpha}{2} \mathbf{e}_{y'} \quad (16)$$

Both the magnetic and electric transition moment of the *A* state are thus found to be directed along the twofold C_2^y axis: this alignment of the two vectors creates a rotatory strength in the transition to the upper state

$$R_j^A = \mathrm{Im}(\mathbf{m}_j^A \cdot \boldsymbol{\mu}_j^A) = \frac{\pi\nu_N \mu_N^2}{2} r_{12} \sin\alpha \quad (17)$$

In a similar way one obtains for the lower *B* state:

$$\boldsymbol{\mu}_j^B = -\sqrt{2}\mu_N \sin\frac{\alpha}{2} \mathbf{e}_{z'} \quad (18)$$

$$\mathbf{m}_j^B = \frac{\pi\imath\nu_N}{\sqrt{2}}(\mathbf{r}_1 \times \boldsymbol{\mu}_1 - \mathbf{r}_2 \times \boldsymbol{\mu}_2)$$

$$= \frac{\pi\imath\nu_N \mu_N}{\sqrt{2}} r_{12} \cos\frac{\alpha}{2} \mathbf{e}_{z'} \quad (19)$$

Both moments are thus directed along the z' direction. The rotatory strength for the lower state is:

$$R_j^B = \mathrm{Im}(\mathbf{m}_j^B \cdot \boldsymbol{\mu}_j^B) = -\frac{\pi\nu_N \mu_N^2}{2} r_{12} \sin\alpha \quad (20)$$

As expected $R_j^A + R_j^B$ obey a zero sum rule. Hence, for the *R* configuration of binaphthyl, one expects in the UV region of the naphthalene B_b band a "normal" CD spectrum with a negative lower branch and a positive upper branch, as is indeed observed.

The long-axis polarized ^1B_b band of naphthalene has a maximum at 45 500 cm^{-1} ($\bar{\nu}_N$); Mason et al. use a transition dipole length of 7 Debye (μ_N).[21] The corresponding oscillator strength is 1.05. Klevens and Platt reported an oscillator strength of 1.70 (to a 49 500 cm^{-1} cutoff)[22] which implies a μ_N value of 8.92 Debye. The center of the two UV bands in TNpPcZn is 45 150 cm^{-1}, which is indeed quite close to $\bar{\nu}_N$. The total oscillator strength is 13.24, or 1.65 per naphthalene, which is in almost quantitative agreement with the broad band *f* of Klevens and Platt. Using the naphthalene characteristics, $\bar{\nu}_N$ = 45 500 cm^{-1} and μ_N = 8.92 Debye, and the geometry for TNpPcMg in Table 3, eqs 17 and 20 predict a rotatory strength for binaphthyl of ±25.3 Debye Bohrmagneton. For a complex with four binaphthyls a total strength of ±101.3 Dμ_B is thus expected. Experimental values for the UV bands in TNpPcZn (see Table 2) are much smaller, +12.6 and −22.8 Dμ_B. This is a typical feature of binaphthyls close to the $\pi/2$ dihedral angle.[21] Since the separation of the two exciton bands is comparable to their bandwidth, the positive and negative branches of the CD signal strongly overlap, which leads to cancellation of rotatory strength. In this respect bianthryls yield better-resolved spectra, which provide more satisfying examples of the exciton coupling model.[20]

5.2 The Circular Dichroism of Monobinaphthyl Phthalocyanine. We now consider the CD that is induced in the Q and Soret bands of Pc by the binaphthyl substituents. The model focuses on an approximate square-planar chromophore, such as CoPc, with one binaphthyl substituent, which is placed on the positive *y* axis. Both the Soret and the Q band correspond to doubly degenerate transitions. They may be decomposed into two components which are respectively symmetric and antisymmetric with respect to the twofold symmetry axis which coincides with the *y* axis. These components may be represented as vectors that are oriented, respectively, along the positive *y* and *x* axis in **4**. An overview of all possible couplings is presented in Figure 10. Because of the long intercenter distance

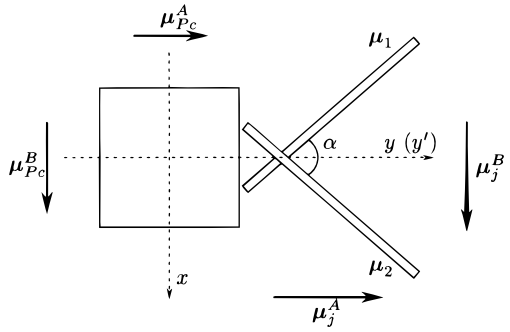

4

R_{12} the interaction between the chromophore and the substituent is not able to significantly lift the degeneracy of the Q and Soret bands. The observed circular dichroism of these transitions will thus correspond to the superposition of the rotatory strengths associated with the two components. If these have opposite signs, a pronounced net CD signal can only be expected if they also show a clear difference in magnitude. A qualitative understanding of the induced CD will thus rely on mechanisms that differentiate between the symmetric and antisymmetric components.

Such differences, indeed, arise on simple symmetry grounds. Selection rules prevent interaction between components having different symmetries with respect to the twofold axis. For this reason, the interaction mechanisms for the *A* and *B* components have to be examined separately. We first take the case of the symmetric transitions, i.e., the ones that are polarized along the *y* direction. Since the corresponding dipoles are aligned, their vector product will be zero, and induction via the coupled oscillator mechanisms remains inactive.

$$R_1^A = 0 \quad (21)$$

In contrast, the CD stealing channel is allowed since the magnetic moment of the *A* transition on the substituent is also aligned along the twofold direction, so that it can couple to the electric transition moment on Pc. The dipole−dipole interaction term for the *A* transitions is given by:

$$V_{ij}^A = -\frac{\sqrt{2}\mu_{Pc}\mu_N}{2\pi\epsilon_0 R_{12}^3} \cos\frac{\alpha}{2} \quad (22)$$

where μ_{Pc} represents the length of one in-plane component of the transition moment on the Pc chromophore. The induced rotatory strength of the *A* component on Pc then reads:

$$R_2^A = \frac{\nu_{Pc}\nu_N \mu_{Pc}^2 \mu_N^2 r_{12}}{2\epsilon_0 h(\nu_N^2 - \nu_{Pc}^2) R_{12}^3} \sin\alpha \quad (23)$$

(21) Mason, S. F.; Seal, R. H.; Roberts, D. R. *Tetrahedron* **1974**, *30*, 1671−1682.

(22) Klevens, H. B.; Platt, J. R. *J. Chem. Phys.* **1949**, *17*, 470−481.

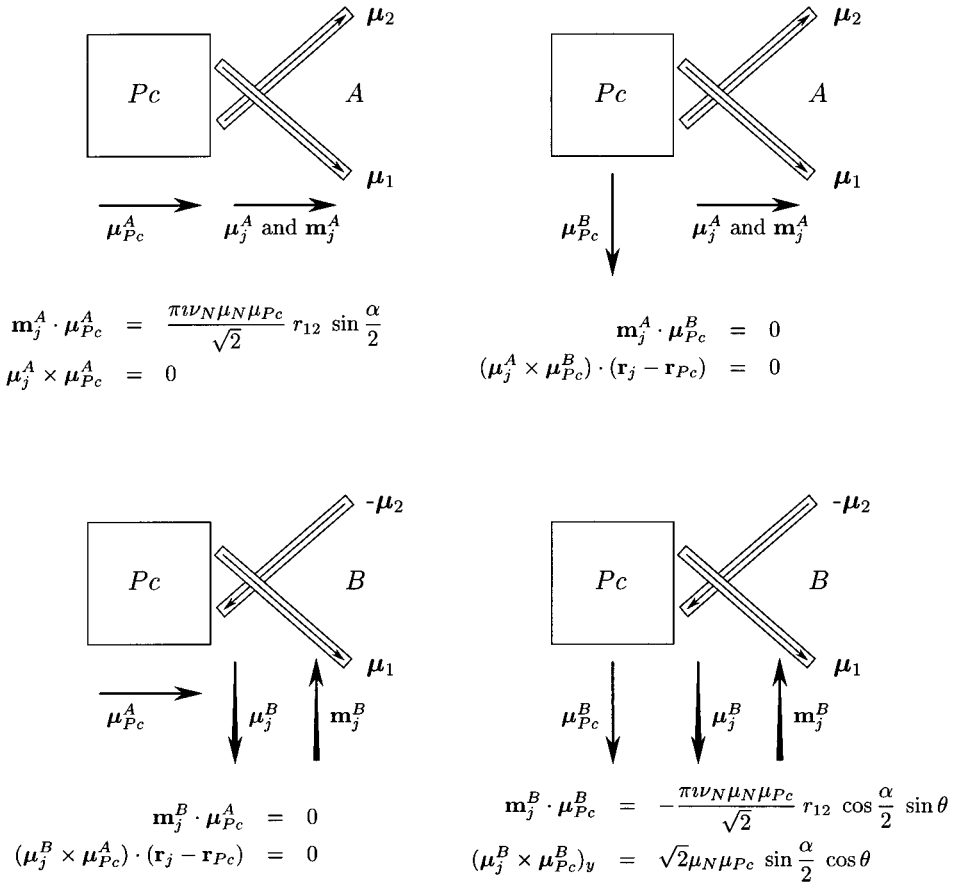

Figure 10. Overview of all possible couplings. All moments are in-plane except for $\boldsymbol{\mu}^B_j$ and $\mathbf{m}^B_j$.

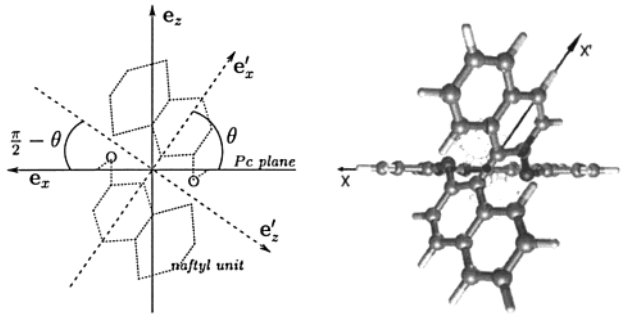

Figure 11. View along the *y* axis.

Note that the transition frequency of the substituent was approximated as ν_N, thus neglecting the exciton splitting of the binaphthyl bands. This expression can be applied both to the Soret and the Q band by inserting the appropriate transition moment, μ_{Pc}, and frequency, ν_{Pc}.

Next we must consider the *B* component. In this case, the geometric relationships between the central and peripheral transitions are different. The central *B* component lies in the plane of the Pc along $\mathbf{e}_x$. The electric transition dipole of *B* type on the subsituent is also perpendicular to the twofold axis, but along $-\mathbf{e}_{z'}$. A view along the *y* direction is shown in Figure 11. The scalar product between these directions can be expressed as

$$\mathbf{e}_x \cdot (-\mathbf{e}_{z'}) = \cos(\pi/2 - \theta) = \sin\theta \tag{24}$$

where θ was given in Table 3. The dipole−dipole interaction term for the *B* transitions then becomes:

$$V^B_{ij} = \frac{\sqrt{2}\mu_{Pc}\mu_N}{4\pi\epsilon_0 R^3_{12}} \sin\frac{\alpha}{2} \sin\theta \tag{25}$$

The vector term in the coupled oscillator mechanism is further obtained as follows:

$$\begin{aligned}(\mathbf{r}_j - \mathbf{r}_i)\cdot(\boldsymbol{\mu}_j \times \boldsymbol{\mu}_i) &= -\sqrt{2}\, R_{12}\, \mu_N\, \mu_{Pc} \sin\frac{\alpha}{2}\, \mathbf{e}_y \cdot [\mathbf{e}_{z'} \times \mathbf{e}_x] \\ &= \sqrt{2}\, R_{12}\, \mu_N\, \mu_{Pc} \sin\frac{\alpha}{2} \cos\theta \end{aligned} \tag{26}$$

Similarly, the scalar product in the CD stealing mechanism is given by

$$\begin{aligned}\boldsymbol{\mu}^B_i \cdot \mathbf{m}^B_j &= \frac{\pi i \nu_N\, \mu_N\, \mu_{Pc}}{\sqrt{2}} r_{12} \cos\frac{\alpha}{2}\, \mathbf{e}_x \cdot \mathbf{e}_{z'} \\ &= -\frac{\pi i \nu_N\, \mu_N\, \mu_{Pc}}{\sqrt{2}} r_{12} \cos\frac{\alpha}{2} \sin\theta \end{aligned} \tag{27}$$

The two mechanisms which contribute to the rotatory strength of the *B* type transitions thus read:

$$R^B_1 = -\frac{\nu_{Pc}\nu_N\, \mu^2_{Pc}\, \mu^2_N}{2\epsilon_0 h(\nu^2_N - \nu^2_{Pc}) R^2_{12}} \sin^2\frac{\alpha}{2} \sin 2\theta \tag{28}$$

$$R^B_2 = \frac{\nu_{Pc}\nu_N\, \mu^2_{Pc}\, \mu^2_N\, r_{12}}{4\epsilon_0 h(\nu^2_N - \nu^2_{Pc}) R^3_{12}} \sin\alpha \sin^2\theta \tag{29}$$

The ratio between the rotatory strengths of the symmetric and

antisymmetric components is only dependent on the geometrical parameters that were listed in Table 3:

$$\frac{R_1^A + R_2^A}{R_1^B + R_2^B} = \frac{2r_{12}\sin\alpha}{-2R_{12}\sin^2\frac{\alpha}{2}\sin 2\theta + r_{12}\sin\alpha\sin^2\theta} \quad (30)$$

If we insert the optimized parameters from Table 3 into this equation, we obtain a ratio which ranges from −2.1 to −3.94 for oxo- and sulphur-bridged substituents, respectively. This means that the two components have different signs, but with the positive *A* branch at least twice as strong as the negative *B* branch. This is because in the *B* component the coupled oscillator and CD stealing mechanisms counteract each other, while the *A* component only gets its strength from the CD stealing term. Hence, the CD spectrum of the Q and Soret bands in mono-(*R*)-binaphthylphthalocyanines is expected to be dominated by the positive branch. For the *S* configuration, the sign is, of course, opposite. This is indeed observed in the CD spectra of mono-(*S*)-binaphthyl substituted Pc complexes reported in ref 4.

5.3 Extension to Polysubstituted Pc Complexes. The model that was developed in the previous section considered a monosubstituted chromophore with nearly degenerate excited states. If more substituents of the same configuration are introduced, the induced circular dichroism is expected to vary in an additive way. Two cases will be discussed: trans disubstitution as in $BNpPcH_2$ and overall tetra substitution as in TNpPcM. In the case of trans substitution, the substituent *j* can be mapped onto the trans substituent, say *k*, by a twofold C_2^z rotation axis perpendicular to the Pc plane, as shown in 5.

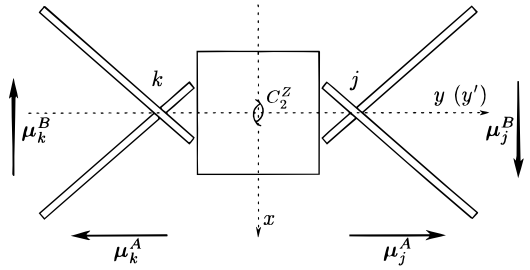

5

We define

$$C_2^z\,\boldsymbol{\mu}_j^A = \boldsymbol{\mu}_k^A \quad (31)$$

$$C_2^z\,\mathbf{m}_j^A = \mathbf{m}_k^A \quad (32)$$

and similarly for the *B* components. The *A* components are aligned along the *y*′ direction, which is perpendicular to the C_2^z axis and, thus, will be antiparallel:

$$\boldsymbol{\mu}_k^A = -\boldsymbol{\mu}_j^A \quad (33)$$

$$\mathbf{m}_k^A = -\mathbf{m}_j^A \quad (34)$$

In contrast, for the *B* components one has:

$$\mathbf{e}_z\cdot\boldsymbol{\mu}_k^B = \mathbf{e}_z\cdot\boldsymbol{\mu}_j^B \quad (35)$$

$$\mathbf{e}_x\cdot\boldsymbol{\mu}_k^B = -\mathbf{e}_x\cdot\boldsymbol{\mu}_j^B \quad (36)$$

The dipole−dipole interaction terms V_{ik}^A and V_{ik}^B will thus have the same magnitude but different signs from their V_{ij}^A and V_{ij}^B counterparts. It is furthermore evident that the position vectors are antiparallel, $\mathbf{r}_k - \mathbf{r}_i = -(\mathbf{r}_j - \mathbf{r}_i)$. If one now introduces these relationships in the expressions for the substituent-induced rotatory strengths, it is found that trans substituents have exactly the same contribution:

$$V_{ik}^B\,(\mathbf{r}_k - \mathbf{r}_i)\cdot(\boldsymbol{\mu}_k^B \times \boldsymbol{\mu}_i^B) = V_{ij}^B\,(\mathbf{r}_j - \mathbf{r}_i)\cdot(\boldsymbol{\mu}_j^B \times \boldsymbol{\mu}_i^B)$$

$$V_{ik}^A\,\mathrm{Im}(\boldsymbol{\mu}_i^A\cdot\mathbf{m}_k^A) = V_{ij}^A\,\mathrm{Im}(\boldsymbol{\mu}_i^A\cdot\mathbf{m}_j^A)$$

$$V_{ik}^B\,\mathrm{Im}(\boldsymbol{\mu}_i^B\cdot\mathbf{m}_k^B) = V_{ij}^B\,\mathrm{Im}(\boldsymbol{\mu}_i^B\cdot\mathbf{m}_j^B) \quad (37)$$

Hence, for the trans disubstituted complexes, the substituent contributions are additive; *trans*-(*R*)-BNpPcM:

$$R_1^A = 0$$

$$R_2^A = \frac{\nu_{Pc}\nu_N\,\mu_{Pc}^2\,\mu_N^2\,r_{12}}{\epsilon_0 h(\nu_N^2 - \nu_{Pc}^2)R_{12}^3}\sin\alpha$$

$$R_1^B = -\frac{\nu_{Pc}\nu_N\,\mu_{Pc}^2\,\mu_N^2}{\epsilon_0 h(\nu_N^2 - \nu_{Pc}^2)R_{12}^2}\sin^2\frac{\alpha}{2}\sin 2\theta$$

$$R_2^B = \frac{\nu_{Pc}\nu_N\,\mu_{Pc}^2\,\mu_N^2\,r_{12}}{2\epsilon_0 h(\nu_N^2 - \nu_{Pc}^2)R_{12}^3}\sin\alpha\sin^2\theta \quad (38)$$

For the tetra-substituted complex with D_4 symmetry, the substituent *j* can be mapped on a substituent in cis position, say *l*, by a fourfold rotation C_4^z around the central upright direction, as shown in **6**.

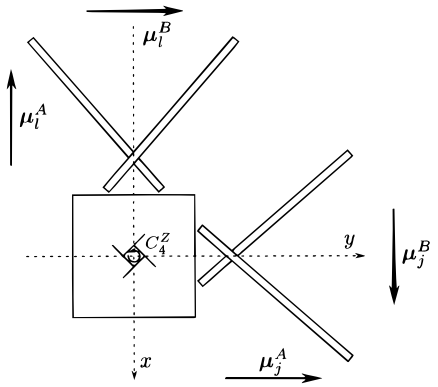

6

One defines

$$C_4^z\,\boldsymbol{\mu}_j^A = \boldsymbol{\mu}_l^A \quad (39)$$

$$C_4^z\,\mathbf{m}_j^A = \mathbf{m}_l^A \quad (40)$$

and similarly for the *B* components. Here, the *j* substituent is, as before, located on the positive *y* direction. The rotated substituent *l* is then positioned along the negative *x* direction. This implies

$$\mathbf{e}_x\cdot\boldsymbol{\mu}_l^A = -\mathbf{e}_y\cdot\boldsymbol{\mu}_j^A \quad (41)$$

$$\mathbf{e}_z \cdot \boldsymbol{\mu}_l^B = \mathbf{e}_z \cdot \boldsymbol{\mu}_j^B \tag{42}$$

$$\mathbf{e}_y \cdot \boldsymbol{\mu}_l^B = \mathbf{e}_x \cdot \boldsymbol{\mu}_j^B \tag{43}$$

and similarly for the components of the magnetic dipoles. From these relations it is clear that the $\boldsymbol{\mu}_l^A$ transition will couple to the central $\boldsymbol{\mu}_i^B$ component, and vice versa $\boldsymbol{\mu}_l^B$ to $\boldsymbol{\mu}_i^A$. The corresponding dipole coupling elements are denoted respectively as V_{il}^A and V_{il}^B. Symmetry implies $V_{il}^A = -V_{ij}^A$ and $V_{il}^B = V_{ij}^B$. The following vector equalities then result:

$$V_{il}^B (\mathbf{r}_l - \mathbf{r}_i) \cdot (\boldsymbol{\mu}_l^B \times \boldsymbol{\mu}_i^A) = V_{ij}^B (\mathbf{r}_j - \mathbf{r}_i) \cdot (\boldsymbol{\mu}_j^B \times \boldsymbol{\mu}_i^B)$$

$$V_{il}^A \, \mathrm{Im}(\boldsymbol{\mu}_i^B \cdot \mathbf{m}_l^A) = V_{ij}^A \, \mathrm{Im}(\boldsymbol{\mu}_i^A \cdot \mathbf{m}_j^A)$$

$$V_{il}^B \, \mathrm{Im}(\boldsymbol{\mu}_i^A \cdot \mathbf{m}_l^B) = V_{ij}^B \, \mathrm{Im}(\boldsymbol{\mu}_i^B \cdot \mathbf{m}_j^B) \tag{44}$$

These equations indicate that the central transition with moment $\boldsymbol{\mu}_i^A$ receives from substituent *l* in cis position exactly the same rotatory strength as its $\boldsymbol{\mu}_i^B$ partner receives from substituent *j*, and vice versa. Since the two partners are degenerate, all the induced strengths are superimposed and again, as a result, the total signal will be additive. One thus expects from a combination of the *cis* and *trans* rules that for a D_4 complex the total induced CD in the Q and Soret regions will be four times as large as for the monosubstituted compound; tetra-(*R*)-TNpPcM:

$$R_1^A = R_1^B = -\frac{\nu_{Pc} \nu_N \mu_{Pc}^2 \mu_N^2}{\epsilon_0 h (\nu_N^2 - \nu_{Pc}^2) R_{12}^2} \sin^2 \frac{\alpha}{2} \sin 2\theta$$

$$R_2^A = R_2^B = \frac{\nu_{Pc} \nu_N \mu_{Pc}^2 \mu_N^2 r_{12}}{\epsilon_0 h (\nu_N^2 - \nu_{Pc}^2) R_{12}^3} \sin \alpha \left(1 + \frac{1}{2} \sin^2 \theta\right) \tag{45}$$

Using these formulae we can estimate the rotatory strength of the Q bands in BNpPcM and TNpPcM (M = Zn, Co). The geometrical input consists of the optimized values for, respectively, $BNpPcH_2$ and TNpPcMg in Table 3. The spectroscopic characteristics of naphthalene are $\mu_N = 8.92$ D and $\nu_N = 1.364 \times 10^{15}\ s^{-1}$, as reported in section 5.1. Finally, the phthalocyanine characteristics were taken from the spectral fits in Table 1. Note that the dipole length μ_{Pc} refers to one degenerate component of the Q(0,0) band. The overall $|\boldsymbol{\mu}|$ values in the table must thus be divided by $\sqrt{2}$ to obtain μ_{Pc}. In Table 4 we present the calculated rotatory strengths and compare them to experimental. There is a clear qualitative agreement which will be discussed in the next section.

6. Discussion

CD signals are delicate marks of electronic structure which are very difficult to calculate by straightforward ab initio methods. Models, as the one we have presented here, should be used primarily to obtain a qualitative understanding of the spectral features. In the present case of a central chromophore which has no intrinsic chirality, symmetry selection rules control induction channels between the central transition and outer chiral substituents. Detailed consideration of the induction mechanisms leads to the correct prediction of the sign of the CD signal in the Q and also Soret bands of Pc with chiral binaphthyl bands. The data in Table 4 indicate that the model also yields a reasonable estimate of the magnitude of the induced CD. The variation of the rotatory strengths in the four metal complexes considered parallels the variation of the oscillator strengths, but the increase of *R* from BNpPcM to TNpPcM is more pronounced than could be expected on the basis of the increase of oscillator strength. The model suggests that slight changes in geometry are mainly responsible for this observation.

Table 4. Estimated Rotatory Strengths for the Q Band in BNpPcM and TNpPcM[a,b]

	BNpPcZn	BNpPcCo	TNpPcZn	TNpPcCo
ν_{Pc} (10^{14} s^{-1})	4.377	4.4	4.257	4.227
μ_{Pc} (D)	5.04	4.15	7.72	5.51
R_1^A (Dμ_β)	0	0	−0.227	−0.115
R_2^A (Dμ_β)	0.331	0.226	0.477	0.240
R_1^B (Dμ_β)	−0.270	−0.183	−0.227	−0.115
R_2^B (Dμ_β)	0.112	0.076	0.477	0.240
$\sum R$ (Dμ_β)	0.173	0.119	0.500	0.250
R_{exp} (Dμ_β)	0.274	0.166	1.719	0.715

[a] Geometrical parameters are taken from Table 3. [b] ν_{Pc} and μ_{Pc} were calculated from the spectral fits in Table 1.

Throughout the foregoing treatment we have assumed that the components of the phthalocyanine transitions be degenerate and oriented along the quantization axes through the substituents. In the protonated phthalocyanine, the central hydrogens can break this symmetry and introduce sizable splittings, especially in the Q band, with components that are polarized along or perpendicular to the interhydrogen axis, see, e.g., in Figure 2. In principle, this symmetry lowering could split the *A* and *B* components and thus resolve the positive and negative branches of the CD spectrum in the Q region, yielding a characteristic derivative-shaped signal. In $BNpPcH_2$, however, the interhydrogen axis makes an angle of 45° with the twofold direction of quantization. This perturbation, which is much stronger than the perturbation from binaphthyl substituents, will thus not resolve the *A* and *B* components but mix them in equal amounts (**7**). As a result, the positive and negative branches of the CD,

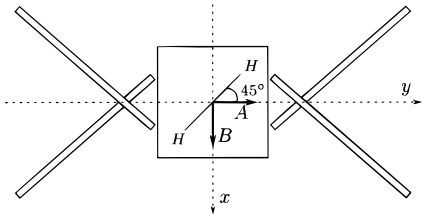

7

associated with the *A* and *B* components, will remain superimposed, and no derivative-shaped signal will appear.

In contrast, in $TNpPcH_2$, the interhydrogen axis coincides with an axis of quantization through the ligands (**8**). The $\boldsymbol{\mu}_i^A$ and $\boldsymbol{\mu}_i^B$ transitions will thus indeed be resolved at different energies, but these components will now carry the same induced CD, because they accumulate rotatory strengths of either sign.

A clear resolution of the induced CD in the Q band region can thus only be achieved in a trans-substituted complex with a pronounced splitting of the Q band, where the polarizations of the chiral induction and the splitting field coincide. This feature is seen to some extent in the spectra of BNpPcZn (Figure 1). Indeed, in contrast to the Q(0,0) band of TNpPcZn (Figure 3), the Q(0,0) band of this complex is not symmetrical and has a peak (686 nm) and a shoulder (∼677 nm), suggesting that it is composed of a superimposition of two slightly split transitions. The similarity of the positions of the MCD trough (689 nm) and peak (678 nm) to this absorption peak and shoulder (Faraday *B* terms) further shows that the actual electronic π system of

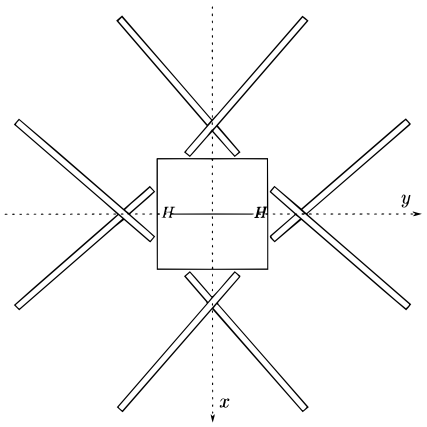

8

BNpPcZn is lower than D_{4h}. Accordingly, we have carried out molecular orbital calculations of 1,11,15,25-tetramethoxyphthalocyaninatozinc(II), which has a similar π conjugated system as that of BNpPcZn (Figure 12), using the ZINDO/S program.[23,24] In the Q band region, two transitions are estimated to lie at 674 ($f = 1.479$) and 671 nm ($f = 1.432$), and these are assigned to the HOMO (a_u) − LUMO (b_{2g}) (B_{2u} symmetry) and the HOMO (a_u) − 2nd LUMO (b_{1g}) (B_{1u} symmetry) transitions, respectively. Accordingly, the Q band to lower energy has polarization along the *y* axis while that to higher energy is polarized along the *x* axis (Figure 12).

Comparison of this result with the overview of possible couplings in Figure 10 indicates that the coupling patterns shown at the top left and bottom right in Figure 10 are associated with the *y*- and *x*-polarized transitions, respectively. The rotatory strengths in the former and the latter transitions are given in eq 38 as the *A* and *B* terms, respectively. The *A* terms can be rewritten as

$$R^A = R_1^A + R_2^A = 2\rho r_{12} \sin \alpha \tag{46}$$

while the *B* terms are simplified into the following form

$$R^B = R_1^B + R_2^B = \rho\left(-2R_{12} \sin^2 \frac{\alpha}{2} \sin 2\theta + r_{12} \sin \alpha \sin^2 \theta\right) \tag{47}$$

where

$$\rho = \frac{\nu_{Pc}\nu_N \mu_{Pc}^2 \mu_N^2}{2\epsilon_0 h(\nu_N^2 - \nu_{Pc}^2)R_{12}^3} \tag{48}$$

which is always positive in sign. Introduction of θ, α, r_{12}, and R_{12} values for BNpPcM in Table 3 into eqs 46 and 47 produces 8.59ρ for R_2^A and -4.11ρ for R_B. Since ρ is positive in sign, these values of rotational strength indicate that the Q band induced CD of BNpPcZn (Figure 1) is expressed as the sum of a large positive rotational strength to the longer wavelength side and a small negative rotational strength to the shorter wavelength side. In the experimental induced CD spectrum (Figure 1), a resolution is not seen, since the splitting of the Q(0,0) band is too small. However, because of the above reasons, the main Q band induced CD peak of BNpPcZn is narrower than the bandwidth of the main absorption Q band (Figure 1).

(23) Ridley, J. E.; Zerner, M. C. *Theor. Chim. Acta* **1973**, *32*, 111−134.

(24) Zerner, M. C.; Loew, G. H.; Kirchner, R. F.; Mueller-Westerhoff, U. T. *J. Am. Chem. Soc.* **1980**, *102*, 589−599. In the calculation, the choice of configuration was based on energetic considerations, and all singly excited configurations up to 7 eV were included.

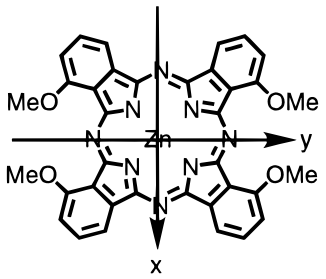

Figure 12. Q band polarization.

Finally, we would like to make some comments on the relative induced CD intensity of the Q (∼550−750 nm) and Soret bands (∼300−450 nm). As seen in Figures 1−3, the apparent intensity (absorption coefficient) of the Soret band in the absorption spectra is always much smaller than that of the Q band, while in the CD spectra the $[\theta]$ values in the Soret region become relatively stronger. This trend is especially obvious in Figures 1 and 2. As shown in eqs 23, 29, 38, and 45, the induced rotational strengths (R^A, R^B) are proportional to $\nu_N\nu_{Pc}/(\nu_N^2 - \nu_{Pc}^2)$, where ν_N and ν_{Pc} are the frequencies of the absorption of naphthalene and phthalocyanine, respectively. Accordingly, the calculated rotational strength, i.e. induced CD intensity, is inversely proportional to the difference between the ν_N^2 and ν_{Pc}^2 values. Since the long-axis polarized, most intense absorption band of naphthalene appears at around 220−225 nm[21,25] and the Q and Soret bands of the phthalocyanine in this work appear at around ∼700 and 370 nm, the observed induced CD intensity should indeed be larger for the Soret band than for the Q band. For example, the theoretical rotational strength ratio for TNpPcZn ($\nu_N = 45\,200$ cm^{-1}, ν_{Pc}(Soret) = 27 200 cm^{-1}, ν_{Pc}(Q) = 14 100 cm^{-1}) is 1.12(the Soret band):0.38(the Q band), reproducing the ∼3(320−500 nm):1(550−750 nm) ratio in experiments.

7. Conclusions

In this paper, we have reported the synthesis and characterization of two and four chiral binaphthyl-linked phthalocyanines. Phthalocyanines with *R* and *S* binaphthyls showed positive and negative induced CD respectively, in the characteristic planar absorptions of the phthalocyanine chromophore. The observed dichroism results from the interplay of two induction paths, which are both strongly geometry-dependent. CD studies thus offer a sensitive tool for studying the ligand environment of these chromophores. It was also demonstrated, both theoretically and experimentally, that the effect is additive. The relative CD intensity relationship between the Soret and Q bands and even the shape of the Q CD band have been rationalized by the proposed model. Finally, we expect a dramatic change from a monotonous to a derivative-shaped signal in trans-disubstituted complexes with a proper alignment of the inner protons.

8. Experimental Section

8.1 Measurement. Electronic absorption spectra were recorded with a Hitachi 330LC spectrometer, and circular dichroism (CD) was measured using a Jasco J-725 spectrodichrometer. Magnetic circular dichroism (MCD) measurements were made with the above spectrodichrometer equiped with a Jasco electromagnet which produced magnetic fields as great as 1.09 T (1 T = 1 tesla) with parallel and antiparallel fields. Their magnitudes were expressed in terms of molar

(25) Kobayashi, N.; Minato, S.; Osa, T. *Makromol. Chem.* **1983**, *184*, 2123−2132.

1. TNpPcM (M = H_2, Zn, Co)

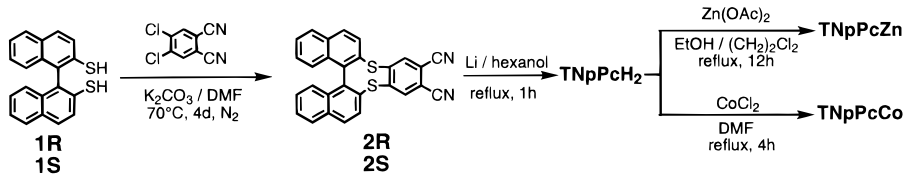

2. BNpPcM (M = H_2, Zn)

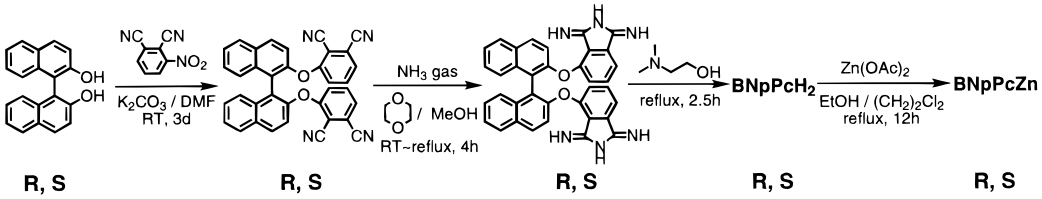

9

ellipticity ([θ]/deg dm^3 mol^{-1} cm^{-1}) for CD and molar ellipticity per tesla ([θ]$_M$/deg dm^3 mol^{-1} cm^{-1} T^{-1}) for MCD. Four hundred megahertz ^{1}H NMR spectra were recorded with a Jeol GSX-400 spectrometer using $CDCl_3$. FTIR spectra were recorded on a Shimadzu FTIR-8100M spectrometer using KBr discs. High-pressure liquid chromatography (HPLC) was conducted on a Shimadzu LC-6AD liquid chromatograph using a Shimadzu SPD-M10A diode array detector.

8.2 Synthesis. Synthetic routes to (*R*)-BNpPcZn and (*R*)- and (*S*)-TNpPcM (M = H_2, Zn, Co) are shown in **9**, although the former (*R*)-BNpPcZn was prepared as described in our previous paper.[4]

(*S*)- and (*R*)-1,2-Dicyano[4,5-*b*]-dinaphtho[2,1-*e*:1′,2′-*g*]-1,4-dithiocine, (2S and 2R). A mixture of (*S*)-1,1′-binaphthalene-2,2′-dithiol (120 mg, 0.38 mmol), 4,5-dichlorophthalonitrile (70 mg, 0.36 mmol) and dry potassium carbonate (260 mg, 1.90 mmol) was stirred in 20 mL of dry dimethylformamide (DMF) at 70 °C for 4 days under nitrogen. The solvent was removed under reduced pressure, the chloroform-soluble products were extracted, and this layer was washed three times with water, dried over anhydrous magnesium sulfate, and filtered. After removing the chloroform under reduced pressure, the residue was purified by silica-gel column chromatography using methylene chloride as the eluent. Evaporation of the solvent, followed by recrystallization from methylene chloride−hexane, gave 90 mg (54%) of white microcrystals of the desired nitrile **2S**. $[\alpha]_D = -14.7$ (*c* 1.0 g/dL, CH_2Cl_2). mp < 200 °C. Anal. Calcd for $C_{28}H_{14}N_2S_2$: C, 75.99; H, 3.19; N, 6.33. Found: C, 75.81; H, 3.20; N, 6.35. IR (KBr, cm^{-1}); 2230 (CN). ^{1}H NMR (ppm, $CDCl_3$); $\delta = 6.7 - 8.1$ (m, 14H, arom). **2R** was similarly obtained. $[\alpha]_D = +14.6$ (*c* 1.0 g/dL, CH_2Cl_2). Anal. Found: C, 75.82; H, 2.87; N, 6.45.

After synthesizing **2S**, unreacted (*S*)-1,1′-binaphthalene-2,2′-dithiol was recovered from the reaction mixture, and the specific rotation was measured ($[\alpha]_D = +84.6°$, *c* 1.0 g/dL, $CHCl_3$). Comparison of this value with that reported previously ($[\alpha]_D = +85.9°$, *c* 1.0 g/dL, $CHCl_3$)[26,27] indicated that racemization did not occur during the reaction.

(*S*)- and (*R*)-Tetrakis(dinaphtho[1,2-*e*:1′,2′-*g*]-1,4-dithiocino)[2,3-*b*; 2′,3′-*k*; 2″,3″-*t*; 2‴,3‴-*c*′]phthalocyanine, (*S*)- and (*R*)-TNpPcH$_2$. A mixture of phthalonitrile **2S** (60 mg, 0.14 mmol) and lithium (6.7 mg, 0.97 mmol) was refluxed in 2 mL of dry hexanol for 1 hour under a nitrogen atmosphere, and the solvent was evaporated under reduced pressure. The residue was loaded on alumina (activity III) and then on gel permeation (Bio-beads SX-1, Bio-rad) columns using chloroform as the eluent. Removal of the chloroform, followed by recrystallization from chloroform−methanol, three times, gave 23 mg (37%) of pure (*S*)-TNpPcH$_2$ as a green powder. Anal. Calcd for $C_{112}H_{58}N_8S_8$: C, 75.90; H, 3.30; N, 6.32. Found: C, 75.79; H, 3.60; N, 6.24. ^{1}H NMR (ppm, $CDCl_3$); $\delta = (-3.8) - (-3.7)$ (s, 2H, pyrrole), 7.4 − 8.1 (m, 56H, arom). In a similar manner, (*R*)-TNpPcH$_2$ was obtained using **2R** as the starting material. Anal. Found: C, 75.31; H, 3.35; N, 6.55.

Unreacted **2S** was recovered, and its specific rotation was measured ($[\alpha]_D = -14.6°$, *c* 1.0 g/dL, CH_2Cl_2). Accordingly, it was concluded that racemization did not occur.

(*S*)- and (*R*)-Tetrakis(dinaphtho[1,2-*e*:1′,2′-*g*]-1,4-dithiocino)[2,3-*b*; 2′,3′-*k*; 2″,3″-*t*; 2‴,3‴-*c*′]phthalocyaninatozinc(II), (*S*)- and (*R*)-TNpPcZn. (*S*)-TNpPcH$_2$ (13 mg, 7.34×10^{-3} mmol) and dry zinc acetate (65 mg, 0.35 mmol) were refluxed in 5 mL of a mixture of ethanol and 1,2-dichloroethane (2:3 v/v) for 12 hours in the dark under nitrogen, and the solvent was evaporated. The residue was applied to alumina (activity III), then to gel permeation (Bio-beads SX-1, Bio-rad) columns using chloroform as the eluent, and recrystallized from chloroform−acetone, three times, to give 6.1 mg (45%) of the desired green powder. Anal. Calcd for $C_{112}H_{56}N_8S_8Zn$: C, 73.29; H, 3.08; N, 6.10. Found: C, 72.52; H, 3.65; N, 5.43. ^{1}H NMR (ppm, $CDCl_3$); $\delta = 7.3 - 8.1$ (m, 56H, arom). (*R*)-TNpPcZn was obtained similarly using (*R*)-TNpPcH$_2$. Anal. Found: C, 73.47; H, 2.82; N, 6.42.

(*S*)- and (*R*)-Tetrakis(dinaphtho[1,2-*e*:1′,2′-*g*]-1,4-dithiocino)[2,3-*b*; 2′,3′-*k*; 2″,3″-*t*; 2‴,3‴-*c*′]phthalocyaninatocobalt(II), (*S*)- and (*R*)-TNpPcCo. A mixture of (*S*)-TNpPcH$_2$ (10 mg, 5.64×10^{-3} mmol) and dry cobalt chloride (50 mg, 0.39 mmol) was refluxed in 1 mL of dry DMF for 4 hours under nitrogen, and the solvent was removed under reduced pressure. The residue was chromatographed using alumina (activity III) and then gel permeation (Bio-beads SX-1, Bio-rad) columns using chloroform−methanol (20:1 v/v) as the eluent. Evaporation of the solvent, followed by recrystallization from chloroform−acetone, twice, gave 5.4 mg (52%) of green powder of (*S*)-TNpPcCo. Anal. Calcd for $C_{112}H_{56}N_8S_8Co$: C, 73.54; H, 3.09; N, 6.13. Found: C, 72.97; H, 3.35; N, 6.46. (*R*)-TNpPcCo was obtained similarly using (*R*)-TNpPcH$_2$. Anal. Found: C, 73.13; H, 3.52; N, 6.44%. After (*R*)-TNpPcCo was obtained, the unreacted (*R*)-TNpPcH$_2$ was recovered from the reaction mixture, and its [θ] at 349 nm was compared with that of the fresh (*R*)-TNpPcH$_2$. Practically no difference was detected in the magnitude of [θ], and therefore, it was concluded that the possibility of racemization is small, if any.

Acknowledgment. Research at Tohoku University was supported by a Grant-in-Aid for Scientific Research on Priority Area “Delocalized Electron Systems” no. 11133206 from the Ministry of Education, Science, Sports, and Culture, Japan and Asahi Glass Foundation. Research at Leuven University was supported by the concerted action scheme of the Flemish Government (Ministerie van het Wetenschapsbeleid).

JA992556W

(26) Fabbri, D.; Delogu, G.; Lucchi, O. D. *J. Org. Chem.* **1993**, *58*, 1748−1750.

(27) Bandarage, U. K.; Simpson, J.; Smith, R. A. J. *Tetrahedron* **1994**, *50*, 3463−3472.